COX-2 mediates tumor-stromal prolactin signaling to initiate tumorigenesis

Yu Zheng[a,1,2], Valentine Comaills[a,1], Risa Burr[a,1], Gaylor Boulay[a,b], David T. Miyamoto[a,c], Ben S. Wittner[a], Erin Emmons[a], Srinjoy Sil[a], Michael W. Koulopoulos[a], Katherine T. Broderick[a], Eric Tai[a], Shruthi Rengarajan[a,b], Anupriya S. Kulkarni[a], Toshi Shioda[a,d], Chin-Lee Wu[a,b], Sridhar Ramaswamy[a,3], David T. Ting[a,d], Mehmet Toner[e,f], Miguel N. Rivera[a,b], Shyamala Maheswaran[a,e], and Daniel A. Haber[a,d,g,4]

[a]Massachusetts General Hospital Cancer Center,Massachusetts General Hospital, Harvard Medical School, Charlestown, MA 02129; [b]Department of Pathology, Massachusetts General Hospital, Harvard Medical School, Boston, MA 02114; [c]Department of Radiation Oncology, Massachusetts General Hospital, Harvard Medical School, Boston, MA 02114; [d]Department of Medicine, Massachusetts General Hospital, Harvard Medical School, Boston, MA 02114; [e]Department of Surgery, Massachusetts General Hospital, Harvard Medical School, Boston, MA 02114; [f]Center for Bioengineering in Medicine, Massachusetts General Hospital, Harvard Medical School, and Shriners Hospital for Children, Boston, MA 02114; and [g]Howard Hughes Medical Institute, Chevy Chase, MD 20815

This contribution is part of the special series of Inaugural Articles by members of the National Academy of Sciences elected in 2018.

Contributed by Daniel A. Haber, January 31, 2019 (sent for review November 19, 2018; reviewed by Corinne Abate-Shen and Carol Prives)

Tumor-stromal communication within the microenvironment contributes to initiation of metastasis and may present a therapeutic opportunity. Using serial single-cell RNA sequencing in an orthotopic mouse prostate cancer model, we find up-regulation of prolactin receptor as cancer cells that have disseminated to the lungs expand into micrometastases. Secretion of the ligand prolactin by adjacent lung stromal cells is induced by tumor cell production of the COX-2 synthetic product prostaglandin E2 (PGE2). PGE2 treatment of fibroblasts activates the orphan nuclear receptor NR4A (Nur77), with prolactin as a major transcriptional target for the NR4A-retinoid X receptor (RXR) heterodimer. Ectopic expression of prolactin receptor in mouse cancer cells enhances micrometastasis, while treatment with the COX-2 inhibitor celecoxib abrogates prolactin secretion by fibroblasts and reduces tumor initiation. Across multiple human cancers, COX-2, prolactin, and prolactin receptor show consistent differential expression in tumor and stromal compartments. Such paracrine cross-talk may thus contribute to the documented efficacy of COX-2 inhibitors in cancer suppression.

COX-2 | prolactin | NR4A | tumor-stromal communication | metastasis

Invasive localized cancers may shed cells into the bloodstream, circulating tumor cells (CTCs), which become trapped in capillary beds within multiple distant organs, ultimately triggering metastatic disease (1, 2). These disseminated tumor cells may persist as nonproliferative single cells within tissues for prolonged periods of time before a subset initiates proliferation and triggers metastatic recurrence. Early microenvironmental signals that support the initiation of proliferation by disseminated cancer cells are poorly understood. Mouse models of tumor dissemination have pointed to multiple growth suppressive-secreted factors such as TGF-β, BMP, and TSP-1 (3–6), as well as a role for immune surveillance (7, 8), in preventing tumor cell outgrowth. However, early tumor cell growth-enhancing signals are not well defined. Identifying such pathways may support the application of "metastatic chemoprevention," particularly in cancers that have a long latency before metastatic recurrence.

Microenvironmental signals that modulate the initial proliferation of a single disseminated cancer cell may be shared by single cells that have undergone transforming genetic events within primary tissues (9). Supporting this notion are clinical studies documenting the effectiveness of COX-2 inhibitors in suppressing both cancer initiation and metastatic recurrence. Both randomized controlled clinical trials and large observational epidemiological studies have demonstrated that the COX-2–selective inhibitor celecoxib, as well as nonsteroidal antiinflammatory drugs (NSAIDs) inhibiting both COX-1 and COX-2, reduces the risk of developing multiple cancers (10–13). Initial studies demonstrated a marked reduction in the development of adenomatous precancerous polyps in carriers of familial polyposis receiving COX-2 inhibitors (11). Subsequent trials in individuals at general population risk for developing cancer demonstrated reductions in multiple invasive malignancies, including colorectal and lung cancers, as well as potential reductions in prostate cancer (11, 14–18). In these studies, efficacy in cancer prevention required at least 5 y of daily treatment and cancer risk reduction was maintained for up to 20 y posttreatment (16). In addition to primary chemoprevention, meta-analyses also indicate significant effects of COX-2 inhibitors in reducing

Significance

The documented efficacy of COX-2 inhibitors in cancer chemoprevention and in suppression of metastasis is predominantly attributed to inflammatory responses, whereas their effects on tumor-stromal interaction are poorly understood. Through single-cell transcriptome analyses in an immune-compromised mouse xenograft model and in vitro reconstitution experiments, we uncover a tumor-stromal paracrine pathway in which secretion by tumor cells of the COX-2 product prostaglandin E2 induces prolactin production by stromal cells, which activates signaling in disseminated tumor cells with upregulated prolactin receptor expression. Analysis of multiple human cancers confirms differential tumor and stromal cell expression of COX-2, prolactin, and prolactin receptor. Together, these findings may provide novel biomarkers to inform the selective application of COX-2 inhibitors and point to additional targets for suppressing metastasis recurrence.

Author contributions: Y.Z., V.C., R.B., S.M., and D.A.H. designed research; Y.Z., V.C., R.B., E.E., S.S., M.W.K., K.T.B., S. Rengarajan, and A.S.K. performed research; G.B., D.T.M., E.T., T.S., C.-L.W., S. Ramaswamy, D.T.T., M.T., and M.N.R. contributed new reagents/analytic tools; Y.Z., V.C., R.B., G.B., B.S.W., M.N.R., S.M., and D.A.H. analyzed data; and Y.Z., V.C., R.B., S.M., and D.A.H. wrote the paper.

Reviewers: C.A-S., Columbia Medical Center; and C.P., Columbia University.

Conflict of interest statement: Massachusetts General Hospital has filed for patent protection for the circulating tumor cell inertial focusing (iChip) technology.

Data deposition: RNA-Seq and CHIP-Seq data that support the findings of this study have been deposited in the Gene Expression Omnibus (GEO) database (accession no. GSE96676).

[1]Y.Z., V.C., and R.B. contributed equally to this work.

[2]Present address: Exploratory Research, Vertex Biopharmaceuticals, Boston, MA 02115.

[3]Present address: Research and Development, Tesaro, Inc., Waltham, MA 02451.

[4]To whom correspondence should be addressed. Email: dhaber@mgh.harvard.edu.

This article contains supporting information online at www.pnas.org/lookup/suppl/doi:10.1073/pnas.1819303116/-/DCSupplemental.

Published online February 28, 2019.

development of metastases following resection of a primary cancer, an effect demonstrated for colorectal and prostate cancers (19). Interestingly, in colorectal cancer, the chemopreventive effects are most striking in reducing tumors that express COX-2 (20) and have mutations in *PIK3CA* (21), which increase phosphatidylinositol 3′-kinase/Akt activity, a known modulator of COX-2–dependent signaling.

The general antiinflammatory effect of NSAIDs and COX-2 inhibitors has led to the assumption that their chemopreventive action may reflect a role for inflammation in enhancing early tumorigenesis. However, a more precise understanding of tumor-stroma–related mechanisms underlying COX-2 cancer chemoprevention is key to try to distinguish potentially beneficial tumor-suppressive pathways from the more global effect of COX-2 inhibitors. Indeed, despite promising epidemiological studies, cancer chemoprevention trials using the COX-2 inhibitor celecoxib were terminated upon the discovery that it also increases the risk for cardiac events, a complication that outweighs its potential benefit in healthy individuals with low cancer risk (22). The pleiotropic effect of the COX-2 synthetic product prostaglandin E2 (PGE2) on multiple proliferative thrombotic and inflammatory pathways presents a major challenge. This may be addressed, in part, by dissecting the PGE2 pathways that directly modulate tumorigenesis and directing inhibitors to patients at high risk of metastatic relapse, where targeting these pathways may have a more favorable risk/benefit profile.

In pursuing an orthotopic mouse prostate cancer model in which CTCs disseminate to distant organs and persist for weeks as nonproliferative single cells before initiating metastatic proliferation, we identified a pathway involving tumor-stromal interaction linking COX-2 to prolactin signaling. We describe a tumorigenesis-enhancing pathway, whereby cancer cells expressing COX-2 secrete PGE2, which, in turn induces secretion of prolactin by stromal fibroblasts. Up-regulation of prolactin receptor by disseminated cancer cells that are initiating proliferation completes a paracrine loop. The potent inhibition of PGE2 synthesis by celecoxib, independent of its effects on immune responses, abrogates this tumor-stromal cross-talk, and may contribute to the documented cancer-suppressive effects of COX-2 inhibitors.

Results

Single-Cell RNA Sequencing of Individual Cancer Cells and Micrometastases in the Lungs. We generated primary orthotopic tumors by inoculation of GFP-luciferase–tagged mouse prostate cancer cells derived from tissue-specific inactivation of *Pten* (CE1-4) (23) into the prostate gland (henceforth, prostate) of immunosuppressed NSG mice (Fig. 1*A* and *SI Appendix*, Fig. S1*A*). These primary mouse tumor-derived cell lines recapitulate androgenic and epithelial features of primary human prostate cancer, and they display broad metastatic potential following orthotopic injection of 1 million cells into the mouse prostate (23). Proliferation of tumor cells within the prostate is evident by live imaging within 2 wk (*SI Appendix*, Fig. S1*A*), and after 6 wk, single tumor cells (STCs) are identified microscopically within multiple tissues, including the lungs [mean = 394 cells per high-power field (hpf)], liver (mean = 54 cells per hpf), bone marrow (mean = 9 cells per hpf), and brain (mean = 1 cell per hpf) (Fig. 1*A* and *SI Appendix*, Fig. S1 *B* and *C*). Only 2.2 ± 2.0% (four of 184) of STCs detected at this early time point (6 wk; STC_6) are positive for the proliferation marker Ki67, and no multicellular lesions are identified in the lung, the most accessible organ for detailed analysis (Fig. 1*A* and *SI Appendix*, Fig. S1*D*). However, in STCs at 9–11 wk ($STC_{9–11}$) after prostate inoculation, the Ki67-positive proliferative fraction of single cancer cells in the lungs increases to 10.8 ± 3.1% (21 of 195 cells) and rare lesions (<0.1% of all scored events) contain 20 or more cells (Fig. 1*A* and *SI Appendix*, Fig. S1*D*). Within these early micrometastases, the proliferative Ki67-positive cellular fraction is 38.2 ± 6.4% (124 of 325 cells) (Fig. 1*A* and *SI Appendix*, Fig. S1*D*). This orthotopic mouse tumor model thus provides a model for time-dependent initiation of metastatic growth.

While single cancer cells isolated from the lungs at the early 6-wk time point are negative for markers of cell proliferation, they are highly proliferative in vitro when collected by trypsin treatment of the whole organ and incubated in standard tissue culture medium. The s.c. inoculation of 10^6 cells from such in vitro-expanded cultures, derived from cancer cells that were nonproliferative in vivo, readily produces tumors in 16 of 16 NSG mice (*SI Appendix*, Fig. S1*E*). Thus, when presented with different environmental signals, apparently quiescent cancer cells that had disseminated to the lungs are competent to proliferate in vitro, and subsequently initiate tumors in vivo.

To trace temporal changes in transcription during early metastatic initiation, we undertook single-cell RNA sequencing (RNA-Seq) of GFP-tagged tumor cells in different tumor compartments: primary cancer cells (n = 29), CTCs isolated by microfluidic capture (24) from blood specimens (n = 12), and individual tumor cells collected at 6 wk (STC_6; n = 20) and at 9–11 wk ($STC_{9–11}$; n = 55). We also isolated the multicellular micrometastatic lesions evident at 9–11 wk, subjecting these to cell dissociation and single-cell RNA-Seq (n = 33) (Dataset S1). Transcriptional profiles of these 149 single cells are shown in Fig. 1*B*. Primary tumor cells are noteworthy for hypoxic and glycolytic signatures (*SI Appendix*, Fig. S2 *A–C*), while one early metastatic lesion (Met1) shows up-regulation of epithelial genes and a second (Met2) has high expression of the growth factor binding proteins IGFBP5 and IGFBP7 (*SI Appendix*, Fig. S2 *D–F*).

The orthotopic mouse tumor model that we established does not allow for resection of the primary tumor; hence, we could not directly trace the evolution of lung micrometastases from initial STCs. The s.c. inoculation of the primary tumor, which does allow for tumor resection, only produced a very small number of STCs, precluding a detailed transcriptional analysis. Thus, we applied a timeline from orthotopic tumor cell inoculation to dissect pathways potentially involved in the emergence of early proliferation among cancer cells disseminated to the lungs. Compared with the homogeneous pattern observed in the universally nonproliferative cells in the lungs at 6 wk following inoculation, single cancer cells isolated from the lungs at 9–11 wk were heterogeneous, and contained two recurrent pathway clusters (gene set enrichment analysis): a proliferative pathway associated with both G1/S and G2/M cell cycle signatures and a pathway involved in cytokine receptor signaling (Fig. 1 *C–E* and *SI Appendix*, Fig. S3 *A–C*). The emergence of a proliferative signature as STCs transition into micrometastases is consistent with the analysis of Lawson et al. (25) and with the increased Ki67 staining fraction evident in single cancer cells isolated at the 9- to 11-wk time point (Fig. 1*A* and *SI Appendix*, Fig. S1 *B–D*). The cytokine signaling signature was confirmed through a hypergeometric pathway analysis (13 of 16 Biocarta pathways, with a false discovery rate of <0.2) (*SI Appendix*, Fig. S3*D*), and it was selected for further analysis since it represents an unexpected association for early progression of cancer cells disseminated to the lungs.

Induced Expression of Prolactin Receptor Increases Micrometastases in the Lungs. Eighteen cytokine and growth factor receptors passed the statistical threshold for differential expression between single cancer cells isolated at the 6-wk versus 9- to 11-wk time point, with *Prolactin receptor* (*Prlr*) being the most abundant (fourfold median induction, grouping 9- to 11-wk single cells and micrometastases compared with 6-wk single STCs and primary tumor cells; P = $1.3e^{-3}$, Benjamini–Hochberg t test) (Fig. 2*A* and *SI Appendix*, Fig. S3*E*). Primary tumor cells express low levels of *Prlr* [mean = 224 reads per million (RPM), range: 0–1,796 RPM], as do 6-wk single cancer cells (mean = 325 RPM, range: 0–2,099 RPM). In contrast, 9- to 11-wk single cancer cells express higher levels of *Prlr* (mean = 679 RPM, range: 0–8,199 RPM), as do micrometastatic cells (mean = 982 RPM, range: 0–5,441 RPM). The fraction of tumor cells expressing >500 RPM of *Prlr* increases from 17.2% (five of 29)

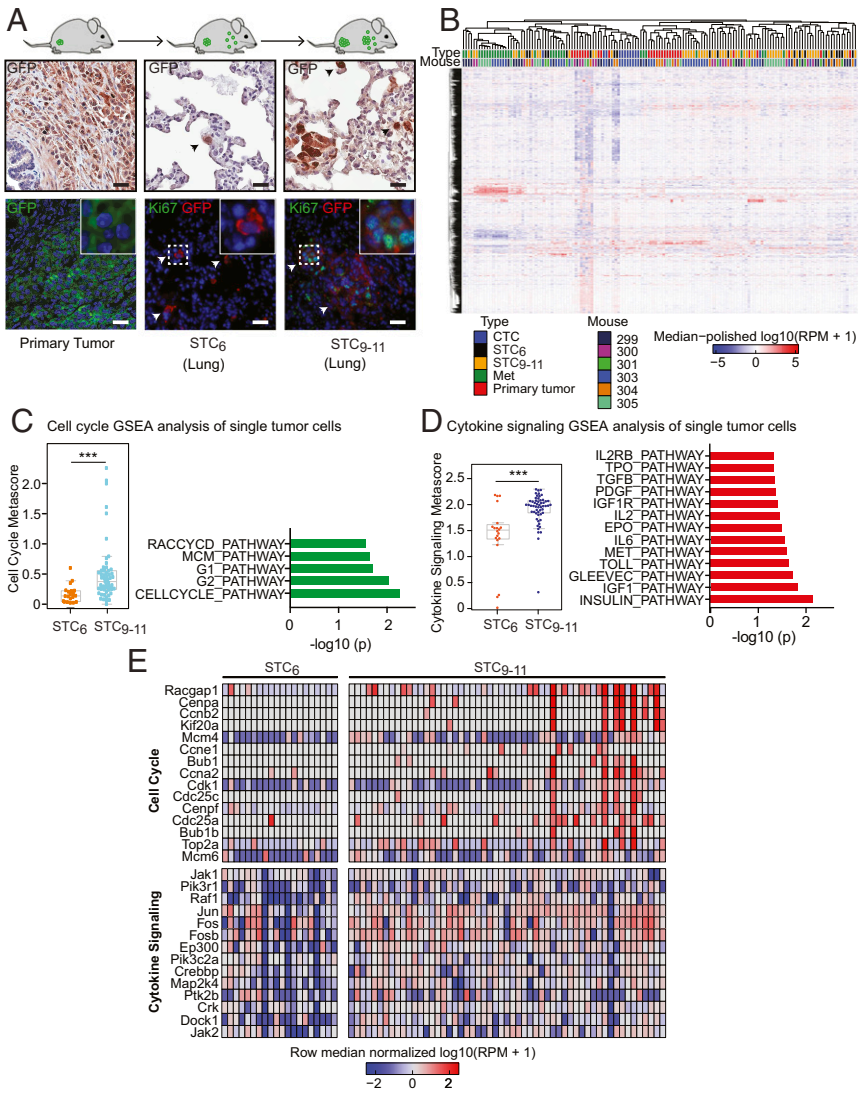

Fig. 1. Single-cell transcriptome profiling of STCs and lung metastases. (*A*) Schematic representation of the orthotopic mouse cancer model, with representative sections of the primary tumor and STCs in the lungs (STC_6 and $STC_{9–11}$) after prostate inoculation. The primary GFP-tagged CE1-4 mouse prostate cancer cells are derived from tissue-specific inactivation of *Pten* in a mouse model (23). Tumor cells are identified by IHC staining for GFP, and proliferative cells are scored by dual-IF staining for GFP and Ki67. (*Insets*: Magnification 3×.) (Scale bars, 25 μm.) (*B*) Unsupervised hierarchical clustering of single-cell RNA-Seq of 149 mouse prostate tumor cells. GFP-tagged primary tumor cells ($n = 29$), CTCs isolated by microfluidic capture (24) from blood specimens ($n = 12$), STCs and fewer than six cell clusters collected from the lungs at STC_6 ($n = 20$) and $STC_{9–11}$ ($n = 55$), and micrometastases evident at 9–11 wk (Met1 and Met2, $n = 33$) were individually micromanipulated and subjected to single-cell RNA-Seq. The genes displayed are the top 2,000 genes with respect to variance across the samples of the RPM values. (*C*, *Left*) Scatter plot showing the cell cycle metascore (G1/S + G2/M) of tumor cells collected from the lungs at STC_6 and $STC_{9–11}$ after orthotopic inoculation (***$P <$ 0.001, two-tailed Student *t* test). (*C*, *Right*) Bar graph showing gene set enrichment for cell cycle pathways in single-cell RNA-Seq of tumor cells collected from the lungs at $STC_{9–11}$ compared with those collected at STC_6 (*x* axis: $-\log_{10}$ of *P* value). (*D*, *Left*) Scatter plot showing the cytokine signaling metascore of STCs collected from the lungs (STC_6 and $STC_{9–11}$) after orthotopic inoculation (***$P < 0.001$, two-tailed Student *t* test). (*D*, *Right*) Bar graph showing gene set enrichment for cytokine pathway clusters based on single-cell RNA-Seq of $STC_{9–11}$ compared with STC_6 (*x* axis: $-\log_{10}$ of *P* value). (*E*) Heat maps of the cell cycle pathway genes (*Top*) and cytokine signaling pathway genes (*Bottom*) up-regulated within $STC_{9–11}$ single cancer cells compared with STC_6 single cancer cells.

in the primary tumor and 20.0% (four of 20) in 6-wk single cancer cells to 34.5% (19 of 55) in 9- to 11-wk single cancer cells and 48.5% (16 of 33) in micrometastasis cell populations, a trend evident in all four independent mice analyzed (Fig. 2*B*). Consistent with RNA-Seq, Prlr protein expression, detected by immunofluorescence (IF), is evident within lung metastases evaluated from multiple mouse models established with three independent *Pten*-null prostate tumor lines (CE1-4, CE1, and CE2) but not in normal lungs (Ctrl) (Fig. 2*C*). As expected, RNA-Seq reveals considerable heterogeneity among single cells, consistent with evolution of both the primary tumor and its metastatic derivatives.

The role of prolactin signaling in tumorigenesis is poorly understood, and given the predominant association between early STC proliferation and *Prlr* expression, we selected this pathway for further analysis. To first test the functional consequences of *Prlr* expression, we generated doxycycline (Dox)-inducible *Prlr* expression in mCherry-tagged CE1-4 cells, which demonstrate Prl-induced activation of downstream signaling (Fig. 2*D*). No such signaling is observed following Dox treatment in the absence of exogenous Prl ligand. Induction of *Prlr* in the presence of ligand has a modest inhibitory effect on cell proliferation in vitro (Fig. 2*E*), and CE1-4 cells expressing the receptor generate primary orthotopic tumors of smaller weight, compared with matched noninduced controls

(mean = 0.47 g for Prlr-induced tumors versus 0.74 g for uninduced controls; $P = 0.04$, two-tailed Student's t test) (Fig. 2 *F* and *G*). The total number of individual cancer cells shed into the lungs by the *Prlr* (Dox)-induced primary tumors is unaltered; however, remarkably, the smaller *Prlr*-induced primary tumors generate a higher number of micrometastatic lesions [for six to 20 cell metastases: mean = 115 (SD ± 10) for *Prlr*-induced versus 44 (SD ± 8) for uninduced controls; $P = 5 \times 10^{-4}$, two-tailed Student's t test; for >20 cell metastases: mean = 68 (SD ± 15) for *Prlr*-induced versus 8 (SD ± 2) for uninduced controls; $P = 2 \times 10^{-3}$, two-tailed Student's t test] (Fig. 2*H*). Micrometastases derived from *Prlr*-induced tumors also display activation of phospho-Erk and phospho-Akt, which is not observed in comparable lesions from noninduced mice (*SI Appendix*, Fig. S4 *A–D*). Thus, prolactin receptor signaling appears to support early micrometastatic outgrowth by single cancer cells that have disseminated to the lungs.

PGE2 Secreted by Tumor Cells Induces Prolactin Expression in Cultured Fibroblasts. Despite up-regulation of *Prlr* in cancer cells that are initiating proliferation in the lungs, single-cell RNA-Seq does not identify mRNA reads for the receptor's ligand, *Prolactin* (*Prl*), in any of these prostate cancer cells. Instead, IF analysis of lung sections shows tumor-associated lung stromal cells with high levels of Prl expression, which is absent in the tumor cells themselves (Fig. 3*A*). Compared with lung tissues from tumor-bearing mice, the normal lung parenchyma from control mice expresses very low levels of Prl, suggesting that colonization by tumor cells is required for its induction in stromal cells (Fig. 3*B*).

To define this potential paracrine signaling pathway in vitro, we first tested multiple human cultured fibroblast and cancer cell lines for *PRL* expression. While human prostate and breast cancer cell lines are negative, all three fibroblast cell lines tested express *PRL* mRNA under baseline culture conditions (Fig. 3*C*). Remarkably, addition of conditioned medium (CM) collected from mouse prostate cancer CE1-4 cells results in a 15- to 120-fold increase in *PRL* expression by the cultured fibroblasts, but not by the tumor cell lines (Fig. 3*D*). The induction of *PRL* mRNA in fibroblasts by tumor cell-derived CM is both time- and dose-dependent (*SI Appendix*, Fig. S5 *A* and *B*), and PRL protein secretion into the culture medium is also evident by quantitation using ELISA (*SI Appendix*, Fig. S5*C*).

To identify the PRL-inducing factor secreted into CM by tumor cells, we took advantage of multiple genetically identical

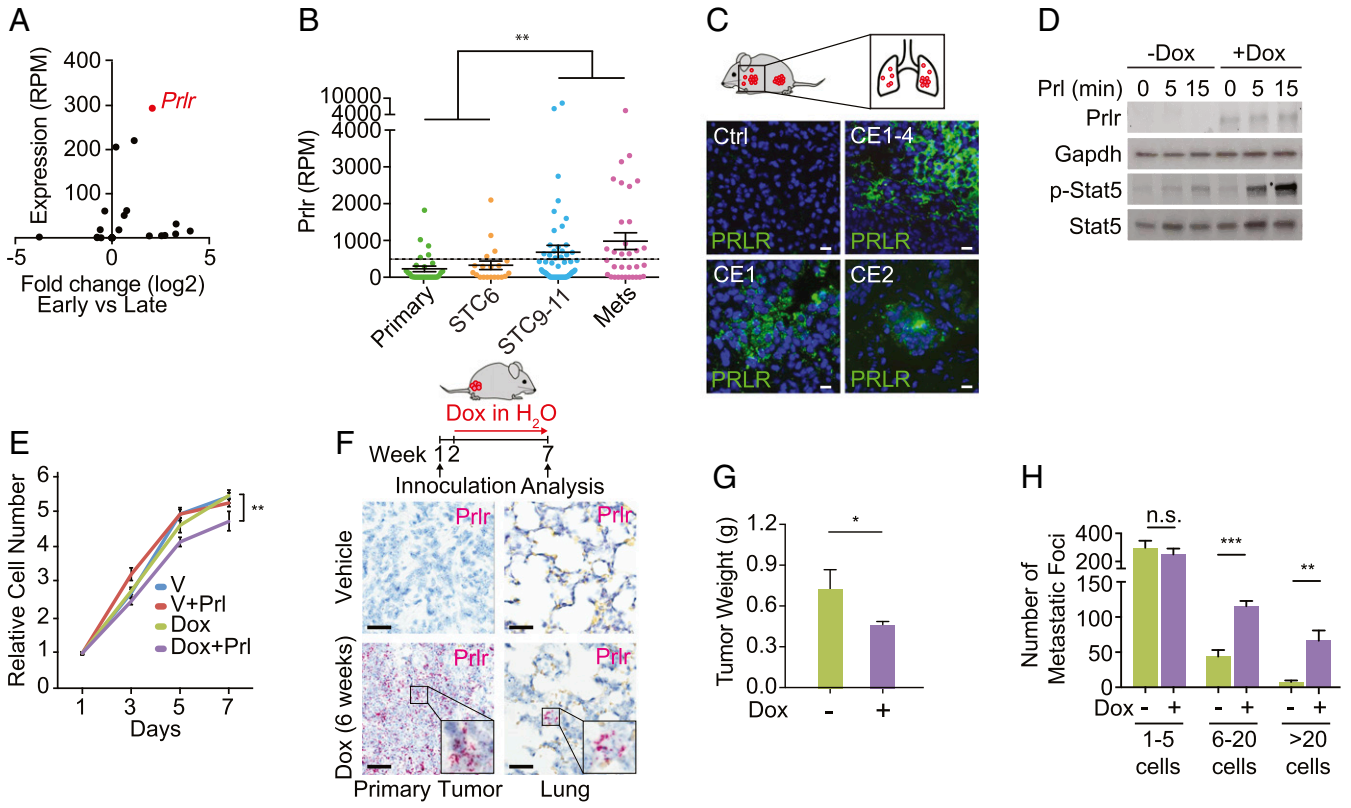

Fig. 2. Prolactin receptor signaling induces metastatic outgrowth. (*A*) Scatter plot showing the median single-cell RNA-Seq expression for cytokine and growth factor receptors (statistical threshold: $P < 0.05$) versus log-twofold change between STCs collected from the primary tumor and lungs after 6-wk orthotopic inoculation (STC_6) versus 9- to 11-wk orthotopic inoculation ($STC_{9–11}$) and micrometastases. *Prlr* is the most abundant differentially expressed receptor. (*B*) Scatter plot showing single-cell RNA-Seq expression of *Prlr* in dissociated primary tumor cells, STCs in the lungs after 6 wk (STC_6) and 9–11 wk ($STC_{9–11}$) of tumorigenesis, and dissociated micrometastases. The dashed line represents the threshold of 500 RPM (**$P < 0.01$, nonparametric Mann–Whitney U test). (*C*) Representative IF images showing the expression of Prlr in lung metastases from three prostate cancer orthotopic mouse models expressing endogenous Prlr, compared with normal lung (Ctrl). (Scale bars, 25 μm.) (*D*) Western blot analyses showing Dox-inducible expression of Prlr in engineered CE1-4 murine prostate tumor cells and activation of its downstream STAT-5 signaling following treatment with 100 ng/mL mouse Prl for 5 or 15 min. (*E*) In vitro growth curves of CE1-4 cells cultured in the presence or absence of Dox to induce Prlr expression, with or without addition of Prl. A modest antiproliferative effect is evident in cells expressing Prlr and treated with Prl (**$P < 0.01$, two-tailed Student t test). V, vehicle. (*F*) Schematic representation of Dox-inducible expression of Prlr within prostate tumors derived from orthotopic injection of CE1-4 cells. In the presence of Dox, *Prlr* is detectable by RNA-ISH within the primary tumor cells, as well as within small micrometastases in the lungs. (Scale bars, 50 μm.) (*G*) Bar graph shows reduced size of the primary tumor following the induction of *Prlr* expression with Dox (+), compared with V-treated controls (–) (*$P < 0.05$, two-tailed Student t test). (*H*) Bar graph shows quantitation of lung tumor foci across different size categories (one to five cells, six to 20 cells, >20 cells) in Dox-induced (+) versus V-treated (–) mice 6 wk after tumor inoculation ($n = 3$ mice per group with at least 10 fields quantified per animal). Post hoc power of 0.16 (***$P < 0.001$, **$P < 0.01$; two-tailed Student t test). n.s., not significant.

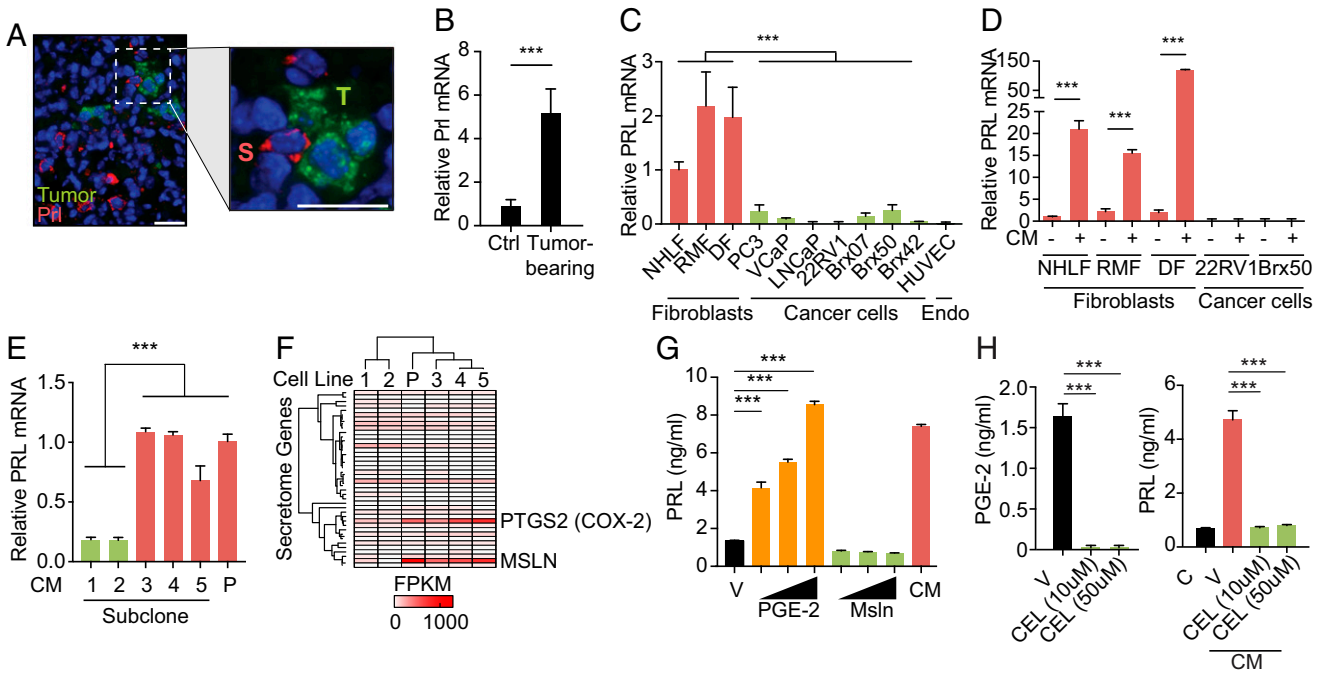

Fig. 3. Paracrine production of prolactin by fibroblasts is induced by tumor-secreted PGE2. (*A*) IF images showing localization of prolactin (Prl) within lung stromal cells (S), but not in adjacent tumor cells (T) marked by mCherry. (Scale bars, 25 μm.) (*Inset*: Magnification: 3×.) (*B*) Bar graph showing expression of *PRL* mRNA in whole-lung samples from healthy control (Ctrl) mice versus those from tumor-bearing mice ($n = 3$ mice per group). Expression is relative to Ctrl mice by qPCR (***$P <$ 0.001, two-tailed Student *t* test). (*C*) Quantitation of basal *PRL* expression in cell lines of different fibroblast lineages [normal human lung fibroblasts (NHLF), human mammary fibroblasts (RMF), and dermal fibroblasts (DF)], prostate cancers (PC3, VCaP, LNCaP, and 22RV1), breast cancer CTC lines (Brx07, Brx50, and Brx42), and endothelial (Endo) cells [human umbilical vein cells (HUVEC)]. *PRL* expression is relative to NHLF (qPCR) (***$P < 0.001$, two-tailed Student *t* test). (*D*) Bar graph showing treatment with CM from CE1-4 tumor cells induces *PRL* mRNA expression in all three fibroblast cell lines, but not in cancer cell lines. *PRL* expression is relative to uninduced levels in NHLF (qPCR) (***$P < 0.001$, two-tailed Student *t* test). (*E*) Quantitation of *PRL* mRNA expression by qPCR in NHLFs treated with CM collected from the parental CE1-4 cell line (P) or from its five subclonal derivatives, showing that CM from subclones 1 and 2 fails to induce *PRL* mRNA. *PRL* expression is relative to P (***$P < 0.001$, two-tailed Student *t* test). (*F*) Heatmap showing 40 secretome-related genes significantly differentially expressed between CE1-4 P and subclones 3–5 (*PRL* inducers) versus subclones 1 and 2 (*PRL* noninducers). Only two transcripts, *COX-2* (*PTGS2*) and *mesothelin* (*MSLN*) show cosegregation with the *PRL* induction phenotype. FPKM, fragments per kilobase of transcript per million. (*G*) Quantitation by ELISA of PRL expression in NHLFs grown in media supplemented with vehicle (V) or with increasing concentrations of PGE2 or Msln. CE1-4–derived CM serves as a positive control. PRL expression is relative to V-treated cells (***$P < 0.001$, two-tailed Student *t* test). (*H, Left*) Bar graph showing the level of PGE2, quantified by ELISA, within the CM of CE1-4 cells treated with V or with 10 μM or 50 μM celecoxib (CEL) (*** $P < 0.001$, two-tailed Student *t* test). (*H, Right*) Bar graph showing PRL expression quantified by ELISA in untreated NHLF [control (C)], following treatment with CM from V-treated CE1-4 cells, or from CE1-4 cells treated with increasing concentrations of CEL (*** $P < 0.001$, two-tailed Student *t* test).

Pten-deficient mouse prostate tumor cell lines whose CM either induces [parental CE1-4 and its subclonal lines 3, 4, and 5] or does not induce (subclonal lines 1 and 2) PRL expression by normal human lung fibroblasts (Fig. 3*E*). Using RNA-Seq, we defined the secretome of these prolactin-inducing versus non–prolactin-inducing cancer cell lines, identifying 40 differentially expressed secretion-related gene products: The top two transcripts highly correlated with *PRL* induction were *COX-2* [prostaglandin-endoperoxide synthase 2 (*Ptgs2*)] and mesothelin (*Msln*) (Fig. 3*F* and *SI Appendix*, Fig. S5*D*). Treatment of fibroblasts with purified Msln has no effect on PRL expression, whereas the synthetic product of COX-2, PGE2, shows a dramatic dose-dependent (fourfold to eightfold) induction of PRL, recapitulating the effect of CE1-4 tumor cell-derived CM (Fig. 3*G*). Moreover, the COX-2 inhibitor celecoxib, which blocks synthesis of PGE2 (26), abolishes the ability of CM from CE1-4 cells to induce PRL in human cultured fibroblasts (Fig. 3*H*). Thus, PGE2 is the main component within prostate cancer cell CM that mediates the induction of PRL by cultured fibroblasts.

PGE2 Induces Orphan Nuclear Receptor 4A-Retinoid X Receptor–Mediated Transcriptional Activation of Prolactin in Fibroblasts. To identify potential mechanisms underlying PGE2-mediated induction of prolactin, we performed both RNA-Seq and genome-wide H3K27-acetylation (H3K27ac) chromatin immunoprecipitation sequencing (ChIP-Seq) using human fibroblasts treated with PGE2 for 6 h. A greater than threefold increase in H3K27ac, a marker associated with increased promoter and enhancer activity (27, 28), is observed at 293 sites across the entire genome, primarily at inter- and intragenic sites (45.7% and 51.5% respectively), with a smaller fraction at transcriptional start sites (2.7%) (Fig. 4 *A* and *B*; $n = 2$ independent experiments). RNA-Seq of PGE2-treated fibroblasts identifies 162 transcripts up-regulated greater than twofold, compared with untreated controls (Fig. 4*C*). Remarkably, in this unbiased genome-wide screen for PGE2 targets, the *PRL* gene is the top hit at the intersection of the RNA-Seq and ChIP-Seq datasets, with 17.19-fold RNA induction after 6 h of PGE2 treatment and dramatic H3K27ac in the gene promoter (Fig. 4 *D* and *E*). Treatment of CE1-4 cancer cells with PGE2 shows no such induction in the *Prl* transcript, consistent with an effect specific to stromal fibroblasts (*SI Appendix*, Fig. S6*A*).

Motif enrichment analysis across all 293 newly acquired H3K27ac sequences identifies consensus DNA binding sites for the orphan nuclear receptor 4A (NR4A) family (29–31) as by far the most significant ($P = 1e^{-77}$; Fig. 4*F*). Remarkably, NR4A binding sites account for 68.6% of all new genome-wide H3K27ac sites acquired following PGE2 treatment (Fig. 4*F*), suggesting that it may constitute the major transcriptional effector of prostaglandin signaling in fibroblasts. The NR4A gene family is composed of three members with a high degree of

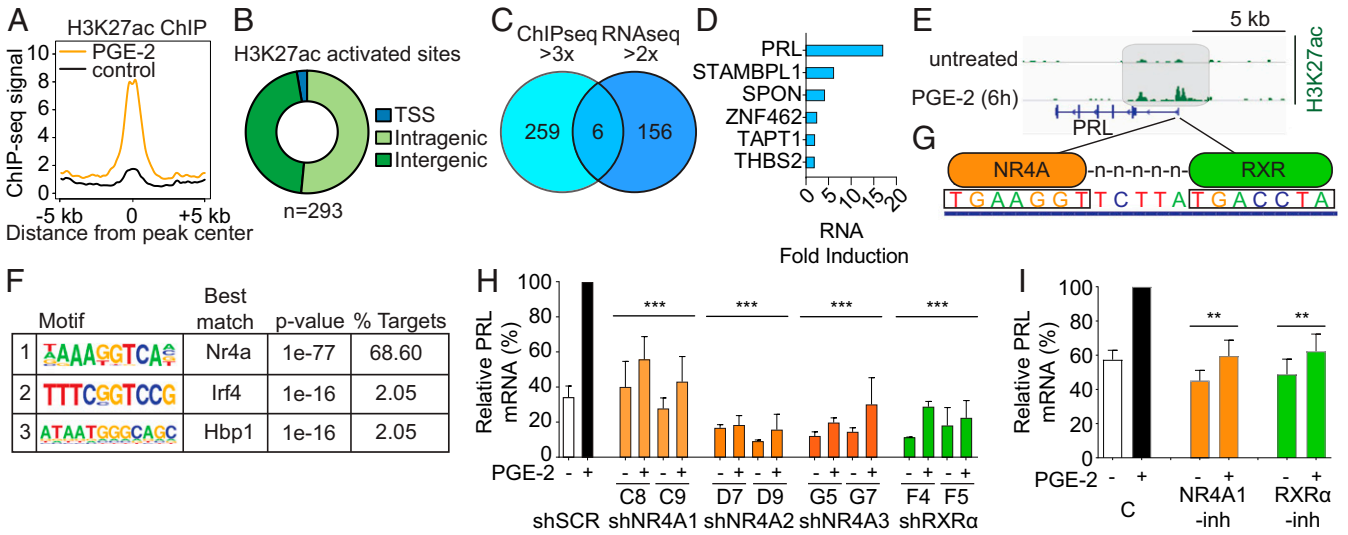

Fig. 4. PGE2-mediated activation of prolactin in fibroblasts is mediated by NR4A-RXR heterodimers. (*A*) Composite plot showing genome-wide H3K27ac ChIP-Seq signals in control (black) and PGE2-treated dermal fibroblasts (DFs; orange). Data represent two biological replicates. The *x* axis represents a 10-kb window centered on increased H3K27ac sites in PGE2-treated cells (10 ng/mL, 6 h; $n = 293$ sites). (*B*) Distribution of increased H3K27ac sites in PGE2-treated DFs among transcriptional start sites (TSS) and intragenic and intergenic genomic loci. Promoters are annotated using the RefSeq promoter database. (*C*) Venn diagram comparing genes with greater than threefold increased H3K27ac activation peaks (ChIP-Seq) and those with greater than twofold up-regulated expression (RNA-Seq) in DFs after 6 h of PGE2 treatment. The 293 H3K27ac sites enriched after PGE2 treatment correspond to 265 unique genes. (*D*) Six genes at the intersection of the ChIP-Seq and RNA-Seq datasets are listed, with prolactin (*PRL*) having the highest fold induction in RNA expression in the RNA-Seq dataset. (*E*) ChIP-Seq data showing increased H3K27ac modification in the promoter region of the *PRL* gene, 6 h after PGE2 treatment of DFs. (*F*) Motif analysis of sites with increased H3K27ac following PGE2 treatment. The motif recognized by NR4A family members (Gene Expression Omnibus accession no. GSM777637) is the most highly enriched and accounts for the majority of sites marked by H3K27ac. (*G*) Nucleotide sequences between the two H3K27ac peaks in the promoter of *PRL* contain a potential DR5 binding site for the NR4A-RXR heterodimer. (*H*) Suppression of *PRL* mRNA induction in DFs by PGE2, following infection with shRNA constructs targeting NR4A1 (C8 and C9), NR4A2 (D7 and D9), NR4A3 (G5 and G7), RXRα (F4 and F5), or scrambled control (shSCR). Baseline and PGE2 (6 h)–induced *PRL* mRNA levels are shown relative to the full induction with shSCR (qPCR). Knockdown efficiency of the relevant lentiviral shRNA constructs against their targets is shown in *SI Appendix*, Fig. S8. Bars are the average of at least two biological replicates. Error bars are 1 SD (***$P < 0.001$; two-tailed Student *t* test; individual comparison with shSCR + PGE2). (*I*) Small-molecule inhibitors suppress PGE2-mediated induction of *PRL* mRNA. Dim-c-pPhCo2Me (10 μM) abrogates NR4A1 (39), while HX531 (1 μM) suppresses RXRα (40). Cells were treated for 18 h before PGE2 exposure. Bars represent the average of at least two biological replicates, normalized to the control PGE2-treated expression for comparison among experiments. Error bars are 1 SD (**$P < 0.01$, two-tailed Student *t* test; individual comparison with control + PGE2). C, control; -inh, inhibitor.

homology and shared DNA consensus binding sites (29, 30); expression of each family member, *NR4A1*, *NR4A2*, and *NR4A3*, is induced at least twofold upon PGE2 treatment of fibroblasts (*SI Appendix*, Fig. S6*B*). These findings are consistent with the modulation of NR4A expression by PGE2 in colorectal cancer cells (32). Analysis of a genome-wide NR4A ChIP-Seq database (33) confirms binding to this specific consensus sequence within the *PRL* promoter (*SI Appendix*, Fig. S6*C*). Of note, the striking PGE2-induced deposition of H3K27ac in the *PRL* promoter resides within a potential DR5 site (34, 35) which includes an NR4A consensus sequence that is separated by five bases from the known NR4A dimerization partner RXR (36) (Fig. 4*G*). Unlike *NR4A*, *RXRα* and *RXRβ* expression is not induced by PGE2 treatment in fibroblasts (*RXRγ* is not expressed in these cells by RNA-Seq) (*SI Appendix*, Fig. S6*D*). Interestingly, NR4A has been linked to expression of prolactin in inflamed joints and in the uterus (37, 38), and our findings now suggest that NR4A-RXR heterodimers constitute key intermediates in the PGE2-mediated induction of prolactin expression in fibroblasts.

To test this model, we first used lentiviral-encoded shRNA constructs to knock down *NR4A* gene family members and *RXRα* in human fibroblasts. Knockdown of *NR4A1*, using either of two shRNA constructs (C8 and C9), suppresses PGE2-mediated *PRL* induction; individual constructs targeting either *NR4A2* (D7 and D9) or *NR4A3* (G5 and G7) abrogate both baseline and PGE2-induced expression of *PRL* (Fig. 4*H*). While the seed sequences targeting each *NR4A* transcript are unique (*SI Appendix*, Fig. S6*E*), coregulation of gene family members appears evident following knockdown of individual genes (*SI Appendix*, Fig. S6*F*), suggesting that all gene family members contribute to *PRL* regulation. Knockdown of *RXRα* (F4 and F5) also dramatically suppresses baseline and PGE2-induced *PRL* expression, consistent with a functional role for the NR4A-RXR heterodimer (Fig. 4*H* and *SI Appendix*, Fig. S6*F*). We also tested the effect of well-characterized small-molecule inhibitors of NR4A1 [Dim-c-pPhCo2Me (39)] and RXRα [HX531 (40)]: Treatment of fibroblasts with either drug suppresses PGE2-mediated induction of *PRL* (Fig. 4*I*). Thus, an unbiased genome-wide screen for all transcriptional and promoter/enhancer (H3K27ac) changes induced by treatment of human fibroblasts with PGE2 identifies *PRL* as a lead transcriptional target, providing independent and orthogonal evidence in support of the PGE2-prolactin pathway uncovered through single-cell analyses in our mouse prostate model (Figs. 1–3). Furthermore, activation of NR4A binding sites is the predominant genome-wide transcriptional consequence of PGE2 treatment in human fibroblasts, and suppression of the NR4A-RXR heterodimer, through either knockdown or small-molecule inhibition, abrogates prolactin induction by PGE2 in these cells.

Tumor-Stromal Expression Patterns of COX-2, Prolactin, and Prolactin Receptor in Primary Human Cancers. The tumor-stromal paracrine signaling involving PGE2, prolactin, and prolactin receptor is evident in multiple independently isolated mouse primary prostate tumor-derived cell lines generated following in vivo *Pten* deletion, and it is also recapitulated in the induction of prolactin by PGE2 in cultured human fibroblasts. To test whether compartmentalized prolactin–prolactin receptor signaling is shared across other tumor types, we used arrayed primary tissue sections

(prostate, colorectal, and lung cancers) to quantify expression of COX-2 (PTGS2), prolactin, and prolactin receptor in human clinical specimens. We used either immunohistochemistry [IHC; Protein Atlas database (41)] staining or quantitative RNA-in situ hybridization (ISH) (branched chain technology RNA-ISH; Advanced Cell Diagnostics, Inc.). High-intensity COX-2 expression is detectable by IHC in the tumor compartment of 12 of 12 prostate cancers [100%; one specimen with low signal (10–30% positive cells) and 11 specimens with high signal (>60% positive cells)], 11 of 11 colorectal cancers (100%; all with high signal), and eight of 12 lung cancers [66.7%; two with low signal, one with intermediate signal (31–59% positive cells), and five with high signal). In all cases, expression of COX-2 is exclusively localized to tumor cells (Fig. 5 and *SI Appendix*, Fig. S7 *A* and *B*). *PRL* mRNA expression has been reported in unfractionated bulk human prostate tumors (42), but using microscopic imaging, we find expression to be largely restricted to the stromal cell compartment; PRL expression is detectable by IHC in 77 of 100 primary and metastatic prostate cancers (77%; 13 with low signal, 15 with intermediate signal, and 49 with high signal), in 24 of 58 colorectal adenomas and cancers (41.4%; 12 with low signal, six with intermediate signal, and six with high signal), and in eight of 11 non-small cell lung cancers (72.7%; three with low signal, two with intermediate signal, and three with high signal) (Fig. 5 and *SI Appendix*, Fig. S7 *A* and *B*). Since expression of the prolactin receptor in human cancers is not well established, we used quantitative RNA-ISH, demonstrating expression of the *PRLR* transcript within tumor cells, but not neighboring stromal cells, in tissue arrays of human primary and metastatic prostate cancers [24 of 89 cases (27%): 11 with low signal, four with

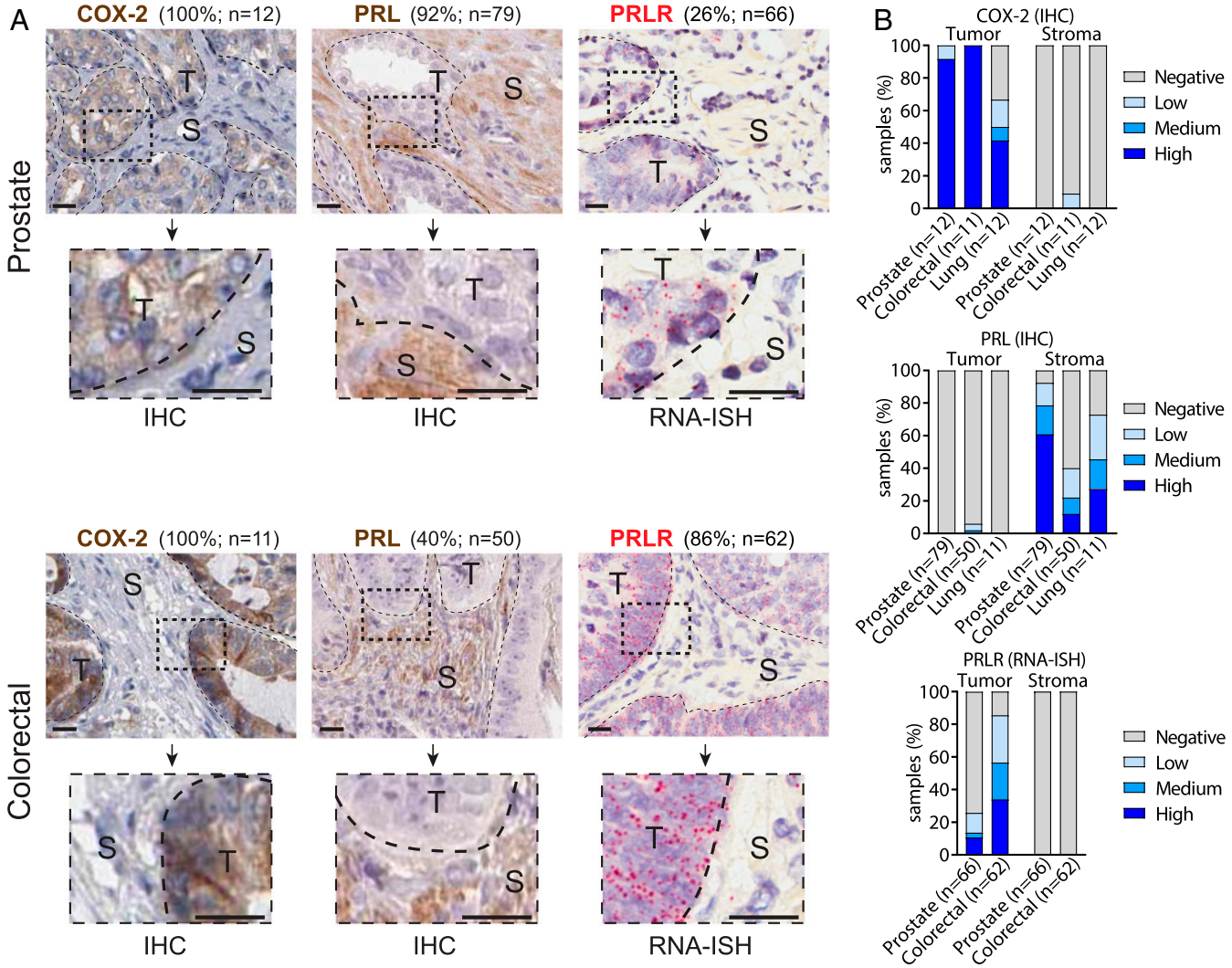

Fig. 5. Localization of COX-2–prolactin signaling components in multiple human cancers. (*A*) Representative images and quantitation of COX-2 (PTGS2) expression in 20 prostate and 24 colorectal human cancers using IHC (proteinatlas.org), with high-magnification images demonstrating expression in the tumor cell compartment. Representative images and quantitation of prolactin (PRL) expression in 12 prostate and 12 colorectal human cancers using IHC (https://www.proteinatlas.org), with high-magnification images showing expression in the stromal compartment. Representative images and quantitation of prolactin receptor (*PRLR*) are shown in 66 prostate and 32 human colorectal cancers, detected using RNA-ISH using the ACD probe against human *PRLR* (542558). S, stromal compartment; T, tumor. (*Insets*) High-magnification images demonstrate transcripts limited to the tumor cell compartment. (Magnification: 3×.) (Scale bars, 20 μm.) Additional tumor types are shown in *SI Appendix*, Fig. S7*A*. (*B*) Bar graphs showing the percentage of human tissue samples positive for COX-2 (PTGS2) and PRL by IHC or for *PRLR* by RNA-ISH, divided into categories of low, medium, and high signal. Samples were considered positive if at least 10% of cells in the appropriate compartment (tumor or stromal) of the section stained positive (10–30% of cells stained was considered low signal, 30–60% of cells stained was considered medium signal, and >60% of cells stained was considered high signal). Tissue samples examined are primary tumors. For PRL staining, data from this study (n = 67) and The Human Protein Atlas (n = 12) were combined (41).

intermediate signal, and nine with high signal], colorectal polyps, and cancers [61 of 84 cases (73%): 26 with low signal, 14 with intermediate signal, and 21 with high signal] (Fig. 5 and *SI Appendix*, Fig. S7 *A* and *B*). Thus, the remarkable pattern of COX-2 and prolactin receptor expression within tumor cell compartments versus prolactin expression in stromal compartments is shared by a large number primary and metastatic human cancers. Finally, we note that a role for the prolactin pathway in tumorigenesis is supported by overexpression of *PRLR* in metastatic, compared with primary prostate tumor, samples ($P = 0.04$; random effects model) (*SI Appendix*, Fig. S7*C*).

Celecoxib Suppresses Mouse Prostate Cancer Initiation in Bone. While the mechanistic basis of celecoxib-mediated cancer chemoprevention in humans as demonstrated in epidemiological studies has not been established, mouse tumor models have shown variable results in recapitulating this effect, depending on tumor types and models, and on the timing of COX-2 inhibition (43–47). Using the mouse prostate tumor model, we first tested the ability of celecoxib to suppress tumor initiation by CE1-4 prostate cancer cells in bone, the primary site of prostate metastasis in humans. Intratibial injection of as few as 250 mouse prostate cancer CE1-4 cells generated tumors detectable by live bioluminescence imaging within 5 wk in eight of 12 (66.7%) injected tibias. Daily treatment of mice with celecoxib (20 mg/kg administered orally daily for 8 wk) starting 1 d before tumor cell inoculation, reduced tumor development to one of 12 (8.3%) injected tibias (odds ratio = 0.045; $P = 0.0094$, Fisher's exact test) (Fig. 6 *A* and *B*). Thus, in cancer cells that appear to recapitulate PGE2-dependent signaling and in the setting of very early tumor initiation from a small cancer cell inoculum, COX-2 inhibition efficiently suppresses the initiation of tumorigenesis in vivo. We next tested the consequences of disrupting this paracrine pathway in our model of prostate cancer metastasis. Starting 1 wk following orthotopic injection of 1 million CE1-4 cells into the prostate, weekly administration of docetaxel (10 mg/kg administered intravenously weekly for 5 wk) reduced the size of primary tumors (from 0.8 to 0.6 g; $P < 0.001$) and the lung metastatic burden for all categories of lesion sizes (*SI Appendix*, Fig. S8). Adding celecoxib (20 mg/kg daily for 6 wk) to docetaxel significantly abrogated the number of metastatic foci in the lungs ($P < 0.001$ for all size categories), while having no effect on the primary tumor (*SI Appendix*, Fig. S8). Importantly, use of this immune-compromised NSG tumor model uncovers a tumor-suppressive effect of COX-2 inhibitors that appears to be mediated through tumor-stromal interactions, independent of the inflammatory effects prominently elicited by PGE2 (48).

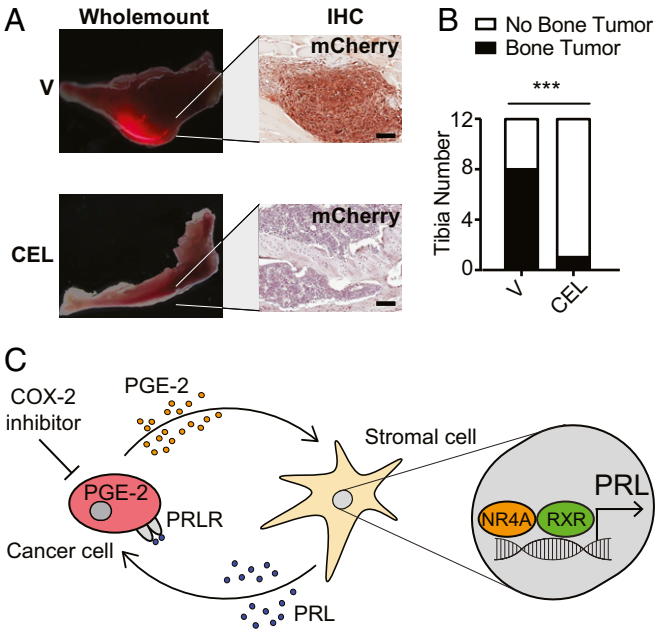

Fig. 6. Functional consequences of Cox-2 inhibition in a prostate mouse model. (*A*) Representative fluorescent whole-mount images of mouse tibia and IHC staining of mCherry-labeled tumor cells from vehicle (V)- or celecoxib (CEL)-treated mice (24-h pretreatment followed by daily treatment with CEL (25 mg/kg, oral) for 8 wk [$n = 6$ mice (12 tibias) per treatment]). (Scale bars, 200 μm.) (*B*) Bar graph showing the occurrence of histologically confirmed tumors in V- versus CEL-treated mice (***$P < 0.001$, Fisher's exact test; odds ratio = 0.045). (*C*) Schematic model illustrating the paracrine signaling network involving PGE2, NRA4-RXR, prolactin, and prolactin receptor in the initiation of tumor growth. PGE2 secretion by cancer cells, through activation of NRA4-RXR binding to *PRL* gene regulatory sequences, induces the production and secretion of prolactin by neighboring stromal fibroblasts. Prolactin, in turn, activates signaling through the prolactin receptor whose expression is up-regulated in tumor cells, thereby promoting their proliferation. This pathway is interrupted by Cox-2 inhibitors (e.g., CEL), which abrogate the initial production of PGE2 in tumor cells.

Discussion

Our data suggest a model whereby secretion of PGE2 by tumor cells induces expression of NR4A family members within neighboring fibroblasts. NR4A-RXR heterodimers bind to the *PRL* promoter, inducing its expression and secretion by fibroblasts. Prolactin then activates signaling in single cancer cells that have up-regulated the prolactin receptor following their dissemination to distant organs, contributing to their expansion into micrometastases (Fig. 6*C*). This pathway, initially based on an orthotopic mouse model of early metastasis, is supported by independent genome-wide analysis of early transcriptional and chromatin changes following treatment of nontransformed human fibroblasts with PGE2. Its clinical relevance is consistent with the striking distinct expression patterns of COX-2 (tumor), prolactin (stroma), and prolactin receptor (tumor) that are evident in a large number of human prostate, colorectal, and lung cancers. Together, these observations implicate a specific paracrine signaling pathway as contributing to the well-established tumor-suppressive effect of the COX-2 inhibitors in human cancer, which has traditionally been attributed to their general antiinflammatory properties. They also suggest a previously unappreciated role for the prolactin pathway in early tumorigenesis, and identify biomarkers and potential therapeutic targets that ultimately may enable more specific targeting of PGE2-mediated enhancement of tumorigenesis.

The orthotopic mouse prostate cancer model that we studied allows for early and large-scale dissemination of STCs to multiple organs, along with a defined period during which these cells remain viable but nonproliferative, before initiating micrometastases. While dormant bone metastases are typical in human prostate cancer, such disseminated cancer cells are evident in multiple organs in various cancer types, and the number of disseminated cancer cells and the ease of isolation from the lungs led us to focus on these cells. Similarly, the frequent expression of COX-2 and prolactin receptor in different human cancer types and the common expression of prolactin itself in tumor-associated stromal cells suggest that this PGE2-driven paracrine pathway may contribute to diverse tumors. Our use of an immunosuppressed mouse model allowed us to identify a tumor-stromal signaling pathway that is distinct from the classical antiinflammatory effects mediated by COX-2 inhibitors. However, we cannot exclude additional contributions to tumor initiation from immune cells as a consequence of PGE2 exposure. In immune-competent models with already established primary tumors, PGE2 has been reported to increase some endogenous antitumor immune responses (48, 49), while reducing therapeutically induced inflammatory responses (50). The relative contributions of immune cells versus stromal fibroblasts to the PGE2 effect in enhancing

the earliest steps in tumor cell proliferation remain to be determined.

In this context, the unbiased genome-wide transcriptional annotation of nontransformed human fibroblasts exposed to PGE2 is remarkable in identifying the *PRL* gene as the major target for such a pleiotropic signaling pathway. NR4A has been identified as a downstream effector of PGE2 in LS-174T colorectal cancer cells (32), and our data extend these findings by identifying NR4A binding sites as the most common chromosomal sites with H3K27ac changes following PGE2 treatment of untransformed fibroblasts (68% of all up-regulated H3K27ac sites). The NR4A pathway itself has been implicated as an intermediate in immune signaling, but its role in normal fibroblasts has not been defined, and its heterodimerization with RXR provides for a degree of complexity and specificity in target gene activation (51). While the PGE2-induced, NR4A-RXR–dependent induction of *PRL* is the most striking transcriptional target of PGE2 identified here, the relative expression patterns of NR4A and RXR family members may lead to additional PGE2 targets in diverse cell types within the cancer microenvironment.

Physiological studies of prolactin have focused on its role as a peptide hormone normally secreted by the pituitary gland and critical to pregnancy-associated lactation (52). However, extrapituitary prolactin, expressed from a distinct promoter, has been reported in bulk unfractionated tumor specimens, including breast and prostate cancers (53–55). The restricted localization of extrapituitary prolactin to the tumor-associated stroma, as opposed to tumor cells, has not been previously appreciated. In addition, prolactin is detectable in blood specimens from patients of both genders with multiple different types of cancers (56), and, recently, it scored as one of the serum proteins most highly correlated with different tumor types in a blood-based multicancer screening platform (57). It is noteworthy, however, that stress and situational anxiety are known to result in marked fluctuations in serum prolactin levels (58), a caveat that will need to be considered in blood-based analyses. At the cellular level, the consequences of prolactin signaling on tumorigenesis are not well established, and diverse effects have been reported following treatment of different cancer cell lines with ectopic prolactin (59–61). In the model that we tested here, prolactin signaling had an inhibitory effect on proliferation of cancer cells, both in vitro and in the primary tumor, but it mediated a striking increase in the ability of single cancer cells that had disseminated to the lungs to produce micrometastases. Understanding the specific prolactin-mediated pathways that underlie this phenomenon may provide additional insight into the early signals that regulate tumor cell dormancy within their microenvironment and the initiation of cancer cell proliferation.

Despite considerable promise in cancer chemoprevention (10–13, 16, 18, 19), COX-2 inhibitors were withdrawn after the discovery that they increase the risk of cardiac events (62), a complication that nullified their potential benefit in healthy individuals at low risk of developing cancer. The application of COX-2 inhibitors to prevent late recurrences of metastatic cancer, following surgical resection of a primary localized but invasive cancer, remains an area of investigation (19). In this context, the risk/benefit profile of COX-2 inhibitors is likely to vary significantly according to both clinical stage and the molecular composition of individual tumors.

Our observations may have clinical implications both in terms of diagnostic biomarkers and potential therapeutic targets in suppressing metastatic recurrence. Future clinical studies will be required to test whether markers of active COX-2–prolactin signaling may identify patients with high-risk primary tumors in whom COX-2 inhibitors could be most effective in preventing metastatic recurrence. In addition, directly targeting key components of the NR4A-RXR signaling pathway might conceivably provide more specificity than COX2 inhibitors, whose suppression of PGE2 synthesis leads to effects on both tumor and cardiovascular systems. Taken together, the dissection of the PGE2-prolactin paracrine signaling axis between the tumor and stroma provides mechanistic insight into pathways that are targeted by COX-2 inhibition, the most compelling and epidemiologically validated chemoprevention strategy in human cancer.

Materials and Methods

Materials, including cell lines and mouse models used and generated by this work, are available in *SI Appendix*. Animal experiments were performed in accordance with institutional guidelines at the Massachusetts General Hospital and approved by the animal protocol (Institutional Animal Care and Use Committee protocol 2010N000006). Human normal and tumor tissue microarrays were generated from discarded excess tissue obtained from the Massachusetts General Hospital (MGH) and after being deidentified per MGH Institutional Review Board-approved protocols (prostate protocol 2000P002109 and colon protocol 2016P002541). Methods used for single-cell collection and in vitro reconstitution experiments are described in *SI Appendix*. Methods for single-cell RNA-Seq, bulk RNA-Seq, ChIP-Seq, IF, IHC, RNA-ISH, qPCR, ELISA, and all associated data analyses are standard and are described in *SI Appendix*. RNA-Seq and CHIP-Seq data that support the findings of the study have been deposited in GEO with the GSE96676 accession code (63).

ACKNOWLEDGMENTS. We thank Dr. V. Deshpande for providing tumor specimens, and L. Libby and R. Desai for technical assistance. This work was supported by grants from the Howard Hughes Medical Institute (to D.A.H.), National Institute of Biomedical Imaging and Bioengineering (Grant EB008047 to M.T. and D.A.H.), National Cancer Institute (Grant 2R01CA129933 to D.A.H.), National Foundation for Cancer Research (D.A.H.), Department of Defense (D.T.M. and D.T.T.), Affymetrix, Inc. (D.T.T.), and Burroughs Wellcome Fund (D.T.T.).

1. Alix-Panabières C, Pantel K (2016) Clinical applications of circulating tumor cells and circulating tumor DNA as liquid biopsy. *Cancer Discov* 6:479–491.
2. Micalizzi DS, Maheswaran S, Haber DA (2017) A conduit to metastasis: Circulating tumor cell biology. *Genes Dev* 31:1827–1840.
3. Massagué J, Obenauf AC (2016) Metastatic colonization by circulating tumour cells. *Nature* 529:298–306.
4. Bragado P, et al. (2013) TGF-β2 dictates disseminated tumour cell fate in target organs through TGF-β-RIII and p38α/β signalling. *Nat Cell Biol* 15:1351–1361.
5. Kobayashi A, et al. (2011) Bone morphogenetic protein 7 in dormancy and metastasis of prostate cancer stem-like cells in bone. *J Exp Med* 208:2641–2655.
6. Gao H, et al. (2012) The BMP inhibitor Coco reactivates breast cancer cells at lung metastatic sites. *Cell* 150:764–779.
7. Malladi S, et al. (2016) Metastatic latency and immune evasion through autocrine inhibition of WNT. *Cell* 165:45–60.
8. Giancotti FG (2013) Mechanisms governing metastatic dormancy and reactivation. *Cell* 155:750–764.
9. Quail DF, Joyce JA (2013) Microenvironmental regulation of tumor progression and metastasis. *Nat Med* 19:1423–1437.
10. Thun MJ, Namboodiri MM, Heath CW, Jr (1991) Aspirin use and reduced risk of fatal colon cancer. *N Engl J Med* 325:1593–1596.
11. Steinbach G, et al. (2000) The effect of celecoxib, a cyclooxygenase-2 inhibitor, in familial adenomatous polyposis. *N Engl J Med* 342:1946–1952.
12. Arber N, et al.; PreSAP Trial Investigators (2006) Celecoxib for the prevention of colorectal adenomatous polyps. *N Engl J Med* 355:885–895.
13. Bertagnolli MM, et al.; APC Study Investigators (2006) Celecoxib for the prevention of sporadic colorectal adenomas. *N Engl J Med* 355:873–884.
14. Smith MR, et al. (2006) Celecoxib versus placebo for men with prostate cancer and a rising serum prostate-specific antigen after radical prostatectomy and/or radiation therapy. *J Clin Oncol* 24:2723–2728.
15. Mason MD, et al.; STAMPEDE Investigators (2017) Adding celecoxib with or without zoledronic acid for hormone-naïve prostate cancer: Long-term survival results from an adaptive, multiarm, multistage, platform, randomized controlled trial. *J Clin Oncol* 35:1530–1541.
16. Rothwell PM, et al. (2011) Effect of daily aspirin on long-term risk of death due to cancer: Analysis of individual patient data from randomised trials. *Lancet* 377:31–41.
17. Flamiatos JF, et al. (2017) Cyclooxygenase-2 (COX-2) inhibition for prostate cancer chemoprevention: Double-blind randomised study of pre-prostatectomy celecoxib or placebo. *BJU Int* 119:709–716.
18. Harris RE, Beebe J, Alshafie GA (2012) Reduction in cancer risk by selective and nonselective cyclooxygenase-2 (COX-2) inhibitors. *J Exp Pharmacol* 4:91–96.
19. Rothwell PM, et al. (2012) Effect of daily aspirin on risk of cancer metastasis: A study of incident cancers during randomised controlled trials. *Lancet* 379:1591–1601.
20. Chan AT, Ogino S, Fuchs CS (2007) Aspirin and the risk of colorectal cancer in relation to the expression of COX-2. *N Engl J Med* 356:2131–2142.
21. Liao X, et al. (2012) Aspirin use, tumor PIK3CA mutation, and colorectal-cancer survival. *N Engl J Med* 367:1596–1606.
22. Funk CD, FitzGerald GA (2007) COX-2 inhibitors and cardiovascular risk. *J Cardiovasc Pharmacol* 50:470–479.

23. Liao CP, et al. (2010) Mouse prostate cancer cell lines established from primary and postcastration recurrent tumors. *Horm Cancer* 1:44–54.
24. Ozkumur E, et al. (2013) Inertial focusing for tumor antigen-dependent and -independent sorting of rare circulating tumor cells. *Sci Transl Med* 5:179ra47.
25. Lawson DA, et al. (2015) Single-cell analysis reveals a stem-cell program in human metastatic breast cancer cells. *Nature* 526:131–135.
26. Penning TD, et al. (1997) Synthesis and biological evaluation of the 1,5-diarylpyrazole class of cyclooxygenase-2 inhibitors: Identification of 4-[5-(4-methylphenyl)-3-(trifluoromethyl)-1H-pyrazol-1-yl]benze nesulfonamide (SC-58635, celecoxib). *J Med Chem* 40:1347–1365.
27. Wang Z, et al. (2008) Combinatorial patterns of histone acetylations and methylations in the human genome. *Nat Genet* 40:897–903.
28. Creyghton MP, et al. (2010) Histone H3K27ac separates active from poised enhancers and predicts developmental state. *Proc Natl Acad Sci USA* 107:21931–21936.
29. Safe S, et al. (2016) Nuclear receptor 4A (NR4A) family–Orphans no more. *J Steroid Biochem Mol Biol* 157:48–60.
30. Maxwell MA, Muscat GE (2006) The NR4A subgroup: Immediate early response genes with pleiotropic physiological roles. *Nucl Recept Signal* 4:e002.
31. Wilson TE, Fahrner TJ, Johnston M, Milbrandt J (1991) Identification of the DNA binding site for NGFI-B by genetic selection in yeast. *Science* 252:1296–1300.
32. Holla VR, Mann JR, Shi Q, DuBois RN (2006) Prostaglandin E2 regulates the nuclear receptor NR4A2 in colorectal cancer. *J Biol Chem* 281:2676–2682.
33. Duren RP, Boudreaux SP, Conneely OM (2016) Genome wide mapping of NR4A binding reveals cooperativity with ETS factors to promote epigenetic activation of distal enhancers in acute myeloid leukemia cells. *PLoS One* 11:e0150450.
34. Forman BM, Umesono K, Chen J, Evans RM (1995) Unique response pathways are established by allosteric interactions among nuclear hormone receptors. *Cell* 81: 541–550.
35. Perlmann T, Jansson L (1995) A novel pathway for vitamin A signaling mediated by RXR heterodimerization with NGFI-B and NURR1. *Genes Dev* 9:769–782.
36. Szanto A, et al. (2004) Retinoid X receptors: X-ploring their (patho)physiological functions. *Cell Death Differ* 11(Suppl 2):S126–S143.
37. Jiang Y, et al. (2011) The orphan nuclear receptor Nur77 regulates decidual prolactin expression in human endometrial stromal cells. *Biochem Biophys Res Commun* 404: 628–633.
38. McCoy JM, et al. (2015) Orphan nuclear receptor NR4A2 induces transcription of the immunomodulatory peptide hormone prolactin. *J Inflamm (Lond)* 12:13.
39. Lee SO, et al. (2014) Diindolylmethane analogs bind NR4A1 and are NR4A1 antagonists in colon cancer cells. *Mol Endocrinol* 28:1729–1739.
40. Konta T, Xu Q, Furusu A, Nakayama K, Kitamura M (2001) Selective roles of retinoic acid receptor and retinoid x receptor in the suppression of apoptosis by all-trans-retinoic acid. *J Biol Chem* 276:12697–12701.
41. Uhlén M, et al. (2015) Proteomics. Tissue-based map of the human proteome. *Science* 347:1260419.
42. Goffin V, Hoang DT, Bogorad RL, Nevalainen MT (2011) Prolactin regulation of the prostate gland: A female player in a male game. *Nat Rev Urol* 8:597–607.
43. Wang D, Fu L, Sun H, Guo L, DuBois RN (2015) Prostaglandin E2 promotes colorectal cancer stem cell expansion and metastasis in mice. *Gastroenterology* 149:1884–1895.e4.
44. Zhang S, et al. (2014) Celecoxib potentially inhibits metastasis of lung cancer promoted by surgery in mice, via suppression of the PGE2-modulated β-catenin pathway. *Toxicol Lett* 225:201–207.
45. DeLong P, et al. (2003) Use of cyclooxygenase-2 inhibition to enhance the efficacy of immunotherapy. *Cancer Res* 63:7845–7852.
46. Williams CS, et al. (2000) Celecoxib prevents tumor growth in vivo without toxicity to normal gut: Lack of correlation between in vitro and in vivo models. *Cancer Res* 60: 6045–6051.
47. Ko CJ, et al. (2017) Inhibition of cyclooxygenase-2-mediated matriptase activation contributes to the suppression of prostate cancer cell motility and metastasis. *Oncogene* 36:4597–4609.
48. Zelenay S, et al. (2015) Cyclooxygenase-dependent tumor growth through evasion of immunity. *Cell* 162:1257–1270.
49. Göbel C, et al. (2014) Functional expression cloning identifies COX-2 as a suppressor of antigen-specific cancer immunity. *Cell Death Dis* 5:e1568.
50. Hou W, Sampath P, Rojas JJ, Thorne SH (2016) Oncolytic virus-mediated targeting of PGE2 in the tumor alters the immune status and sensitizes established and resistant tumors to immunotherapy. *Cancer Cell* 30:108–119.
51. Mangelsdorf DJ, Evans RM (1995) The RXR heterodimers and orphan receptors. *Cell* 83:841–850.
52. Bole-Feysot C, Goffin V, Edery M, Binart N, Kelly PA (1998) Prolactin (PRL) and its receptor: Actions, signal transduction pathways and phenotypes observed in PRL receptor knockout mice. *Endocr Rev* 19:225–268.
53. Ben-Jonathan N, Mershon JL, Allen DL, Steinmetz RW (1996) Extrapituitary prolactin: Distribution, regulation, functions, and clinical aspects. *Endocr Rev* 17:639–669.
54. Li H, et al. (2004) Activation of signal transducer and activator of transcription 5 in human prostate cancer is associated with high histological grade. *Cancer Res* 64: 4774–4782.
55. McHale K, Tomaszewski JE, Puthiyaveettil R, Livolsi VA, Clevenger CV (2008) Altered expression of prolactin receptor-associated signaling proteins in human breast carcinoma. *Mod Pathol* 21:565–571.
56. Sethi BK, Chanukya GV, Nagesh VS (2012) Prolactin and cancer: Has the orphan finally found a home? *Indian J Endocrinol Metab* 16(Suppl 2):S195–S198.
57. Cohen JD, et al. (2018) Detection and localization of surgically resectable cancers with a multi-analyte blood test. *Science* 359:926–930.
58. Armario A, Marti O, Molina T, de Pablo J, Valdes M (1996) Acute stress markers in humans: Response of plasma glucose, cortisol and prolactin to two examinations differing in the anxiety they provoke. *Psychoneuroendocrinology* 21:17–24.
59. Ginsburg E, Vonderhaar BK (1995) Prolactin synthesis and secretion by human breast cancer cells. *Cancer Res* 55:2591–2595.
60. Schroeder MD, Symowicz J, Schuler LA (2002) PRL modulates cell cycle regulators in mammary tumor epithelial cells. *Mol Endocrinol* 16:45–57.
61. Goffin V, Bernichtein S, Touraine P, Kelly PA (2005) Development and potential clinical uses of human prolactin receptor antagonists. *Endocr Rev* 26:400–422.
62. Solomon SD, et al.; Adenoma Prevention with Celecoxib (APC) Study Investigators (2005) Cardiovascular risk associated with celecoxib in a clinical trial for colorectal adenoma prevention. *N Engl J Med* 352:1071–1080.
63. Zheng Y, et al. (2019) COX-2 mediates tumor-stromal prolactin signaling to initiate tumorigenesis. Gene Expression Omnibus (GEO). Available at https://www.ncbi.nlm.nih.gov/geo/query/acc.cgi?acc=GSE96676. Deposited March 15, 2017.